

## Highlights

### **A general representation of the heterogeneous Leader-based Connected Automated Vehicle platoon and stability analyses considering multiple delays**

Tiancheng Ruan,Hao Wang,Linjie Zhou,Yujia Chen,Changyin Dong

- A general representation of the heterogeneous Leader-based CAV platoon as a state delay system is proposed considering multiple delays.
- A novel and more unconservative stability condition of the CAV platoon is derived under the general representation proposed.
- A comprehensive performance evaluation analysis of the four typical Leader-based IFTs is performed in a variety of scenarios.

# A general representation of the heterogeneous Leader-based Connected Automated Vehicle platoon and stability analyses considering multiple delays

Tiancheng Ruan<sup>a,b,c</sup>, Hao Wang<sup>a,b,c,\*</sup>, Linjie Zhou<sup>a,b,c</sup>, Yujia Chen<sup>a,b,c</sup> and Changyin Dong<sup>a,b,c</sup>

<sup>a</sup>Jiangsu Key Laboratory of Urban ITS, Southeast University, 2 Si Pai Lou, Nanjing, 210096, P.R. China

<sup>b</sup>Jiangsu Province Collaborative Innovation Center of Modern Urban Traffic Technologies, 2 Si Pai Lou, Nanjing, 210096, P.R. China

<sup>c</sup>School of Transportation, Southeast University, 2 Si Pai Lou, Nanjing, 210096, P.R. China

## ARTICLE INFO

**Keywords:**

Connected Automated Vehicle (CAV)  
CAV platoon  
General modeling of CAV platoon  
Stability analyses  
State delay system

## ABSTRACT

Urged by the potential of Connected Automated Vehicles (CAVs), research has recently focused on studying their benefits on safety, emissions, and capacity. However, in most works, the CAV has been studied in isolation, and there is a lack of in-depth research on stability conditions. Therefore, this paper proposes a general representation of the heterogeneous Leader-based CAV platoon considering multiple delays. Moreover, a novel and more unconservative stability condition of the CAV platoon is derived under the general representation proposed based on the Lyapunov-Krasovskii Stability Theorem and Bessel-Legendre inequalities. Furthermore, a comprehensive performance evaluation analysis of the four typical Leader-based information flow topologies (IFTs) is conducted to test tracking performance and safety conditions by numerical analyses. The results show that the CACC platoon has superior tracking performance in various scenarios if stability is guaranteed. Moreover, bi-directional communication that receives more information in most cases enables better safety condition for hard braking maneuver situations.

## 1. Introduction

Since the invention of the automobile over a century ago, automotive engineers have been committed to providing safer and more comfortable services. However, traffic problems such as traffic congestion, traffic accidents, and pollutant emissions have become increasingly prominent in past decades with the development of technology (Schrank et al., 2012; Jin and Orosz, 2016). Traditional traffic engineering relies on external measures such as traffic management, traffic control, and so forth to improve traffic capacity and service levels. Nevertheless, these methods are inherently inefficient to satisfy the ever-growing traffic demand. By studying the dynamic and static characteristics of traffic flow, it can be found that the extensive heterogeneity of human factors causes the uncertainty in road traffic (Zhong et al., 2020; Ye and Yamamoto, 2018; van Arem et al., 2016; Yu et al., 2021), which worsens traffic flow stability and restricts capacity.

Fortunately, Automated Vehicle (AV) stands out as a promising enabler and has gained significant popularity in academia and the automotive industry in recent years. It tracks the predecessor based on on-board sensory devices to maintain a constant gap/time gap and becomes increasingly available as standard equipment in modern commercial vehicles with the market penetration rate (MPR) increasing (Wilson and Ward, 2011). Despite its relatively short history, plentiful research has demonstrated its advantages regarding safety, emissions, and capacity over human drivers (Wang et al., 2019; Sarker et al., 2019; Dey et al., 2015).

However, AV is inadequate to fully liberate the potential of autonomous driving. Thanks to the development of Cellular vehicle-to-everything (C-V2X) and wireless communication technology, Connected Automated Vehicle (CAV) emerges by using Vehicle-to-Infrastructure (V2I)/Vehicle-to-Vehicle (V2V) communication to further improve safety and capacity. CAV has the potential to achieve more complex controls compared to AV due to its ability to obtain more adequate and timely information through communication (Navas and Milanés, 2019; Ruan et al., 2021;

\*Corresponding author

 ruantiancheng@seu.edu.cn (T. Ruan); haowang@seu.edu.cn (H. Wang); 220193107@seu.edu.cn (L. Zhou); chenyujia@seu.edu.cn (Y. Chen); dongcy@seu.edu.cn (C. Dong)

ORCID(s):

Zhou et al., 2021). Moreover, CAVs can achieve system optimization rather than user equilibrium by forming a CAV platoon, which can maximize the gain brought by CAVs compared to traditional transportation (Firooznia et al., 2017; Hu et al., 2021).

There has been extensive research on CAV, including exploring its gain for capacity (Ghiasi et al., 2017; Chang et al., 2020), stability (Zhou et al., 2019; Montanino and Punzo, 2021), eco-driving (Qin et al., 2018; Ruan et al., 2022), and designing control strategies of CAVs (Zhu et al., 2019; Chen et al., 2021). However, the modeling object in existing research is only one CAV (Wei et al., 2017; Navas et al., 2016; Milanés and Shladover, 2014) or a specific information flow topology (IFT) for specific research goals (Wang et al., 2021; Chin et al., 2015), which ignores the needs and potential of the CAV platoon as a modeling object. Besides, as for the stability analyses, some studies focus only on string stability and ignore stability by assuming that the CAV platoon is local stable (Stüdli et al., 2017; Wang et al., 2018), while others study the local stability of one CAV (Zhou and Ahn, 2019; Monteil et al., 2019). The former strategy is correct to a certain extent if the communication delay is ignored. However, the communication delay cannot be ignored in practice which means it is necessary to consider the communication delay when exploring the stability condition. As for the latter strategy, the stability condition is derived based on Routh-Hurwitz stability criterion or Lyapunov second method in most research. However, the results obtained based on this method are conservative and underperformed in the state delay system. Therefore, modeling the generalized CAV platoon and developing a novel stability approach with less conservativeness need to be conducted for further analyses.

To fill the gap, this paper proposes a general representation of the heterogeneous Leader-based CAV platoon and a stability condition of the CAV platoon based on the general representation. To sum up, the main contribution of the paper is threefold:

1. A general representation of the heterogeneous Leader-based CAV platoon as a state delay system is proposed considering multiple delays.
2. A novel and more unconservative stability condition of the CAV platoon is derived under the general representation proposed based on the Lyapunov-Krasovskii Stability Theorem and Bessel-Legendre inequalities.
3. A comprehensive performance evaluation analysis of the four typical Leader-based IFTs is performed to reveal tracking performance, transient response, and safety conditions in a variety of scenarios.

The remainder of the paper is outlined as follows: Section 2 introduces the mathematical background, including graph theory and primary matrix inequalities. Section 3 presents the problem statement and a general representation of the heterogeneous Leader-based CAV platoon. Corresponding stability analyses and the derivation of stability conditions based on the Lyapunov-Krasovskii Stability Theorem are carried out in Section 4. Section 5 proposes a comprehensive performance evaluation analysis of the four typical Leader-based IFTs. We summarize the study in Section 6.

**Notations:** Throughout the paper  $\mathbb{R}^n$  denotes the n-dimensional Euclidean space with Euclidian norm  $|\cdot|$  while the set of all  $m \times n$  real matrices is denoted by  $\mathbb{R}^{m \times n}$ . The sets  $\mathbb{S}_n$  and  $\mathbb{S}_n^+$  mean the set of symmetric and symmetric positive definite matrices of  $\mathbb{R}^{n \times n}$ , respectively. The transpose of a vector or a matrix  $A$  is denoted by  $A^T$ . The symmetric matrix  $\begin{bmatrix} A & B \\ * & C \end{bmatrix}$  denotes  $\begin{bmatrix} A & B \\ B^T & C \end{bmatrix}$ . Besides, for any square matrix  $A \in \mathbb{R}^{n \times n}$ , we define  $He(A) = A + A^T$ .  $I_n$  defines the identity matrix of  $n \times n$  dimension while  $0_{m,n}$  stands for the zero matrix of  $m \times n$  dimension. For any matrix  $A \in \mathbb{R}^{n \times n}$ , the notation  $A > 0$  denotes that  $A$  is symmetric and positive definite. The set of continuous functions from an interval  $[-h, 0] \subset \mathbb{R}$  to  $\mathbb{R}^n$  which are, consequently, square integrable is denoted as Banach space  $C([-h, 0], \mathbb{R}^n)$ . For any function  $f \in C$ , the uniform norm  $|f|_h$  refers to  $\sup_{\theta \in [-h, 0]} |f(\theta)|$ .  $diag\{a_1, a_2, \dots, a_n\}$  stands for the diagonal matrix

$$\begin{bmatrix} a_1 & 0 & 0 \\ 0 & \ddots & 0 \\ 0 & 0 & a_n \end{bmatrix}$$
 whose diagonal elements starting at the upper left corner are  $a_1, a_2, \dots, a_n$ . The notation  $\binom{k}{l}$

defines the binomial coefficients given by  $\frac{k!}{(k-l)!l!}$ . Moreover,  $\langle f, g \rangle$  presents the inner product for  $\forall f, g \in C$ .

Let  $A \in \mathbb{R}^{m \times n}$  and  $B \in \mathbb{R}^{p \times q}$ , then  $A \otimes B$  is the Kronecker product of  $A$  and  $B$ :

$$A \otimes B = \begin{bmatrix} a_{11}B & \cdots & a_{1n}B \\ \vdots & \ddots & \vdots \\ a_{m1}B & \cdots & a_{mn}B \end{bmatrix} \in \mathbb{R}^{mp \times nq}$$

Let  $C \in \mathbb{R}^{m \times n}$  and  $D \in \mathbb{R}^{m \times n}$ , then  $C \circ D$  is the Hadamard product of  $C$  and  $D$ :

$$C \circ D = \begin{bmatrix} c_{11}d_{11} & \cdots & c_{1n}d_{1n} \\ \vdots & \ddots & \vdots \\ c_{m1}d_{m1} & \cdots & c_{mn}d_{mn} \end{bmatrix} \in \mathbb{R}^{m \times n}$$

## 2. Mathematical preliminaries

Before providing analyses, we introduce some primary mathematical preliminaries first.

### 2.1. Network model

By regarding each vehicle in the platoon as a node and intervehicle communication as an edge, the information flow topology (IFT) among the platoon can be modeled as a weighted directed graph (digraph)  $\mathcal{G} = \{\mathcal{V}, \mathcal{E}, \mathcal{A}\}$ , in which  $\mathcal{V} = \{1, 2, \dots, n\}$  is the set of nodes and  $\mathcal{E} \subseteq \mathcal{V} \times \mathcal{V}$  is the set of edges. Besides, the weighted adjacent matrix with nonnegative elements is defined as  $\mathcal{A} = [a_{ij}]_{n \times n}$  with  $a_{ii} = 0$  which denotes that the self-edges  $(i, i)$  is not allowed unless indicated otherwise. The edge  $(i, j)$  in  $\mathcal{E}$  means the vehicle  $i$  can communicate with vehicle  $j$  associated with weighted  $a_{ij}$ . Defining the degree matrix of  $\mathcal{G}$  as  $\mathcal{D} = \text{diag}\{d_1, d_2, \dots, d_n\}$ , with  $d_i = \sum_{j \in \mathcal{V}} a_{ij}$ . Therefore, the Laplacian matrix  $\mathcal{L}$  of the weighted digraph  $\mathcal{G}$  can be defined as  $\mathcal{L} = \mathcal{D} - \mathcal{A}$ . It should be noted that the heterogeneity referred to herein is the heterogeneity of the control gains employed by different CAVs.

### 2.2. Stability of state delay system

Consider a linear state delay system described by:

$$\begin{cases} \dot{x}(t) = Ax(t) + A_d x(t-h), & \forall t \geq 0, \\ x(t) = \phi(t), & \forall t \in [-h, 0], \end{cases} \quad (1)$$

where  $x(t) \in \mathbb{R}^n$  is the state vector;  $\phi$  stands for the initial conditions;  $A$  and  $A_d$  are constant matrixes;  $h$  denotes the known constant time delay.

In the context of the stability analysis of state delay systems, the Lyapunov-Krasovskii Stability Theorem is a well-known approach extending the second Lyapunov method dedicated to stability analysis (Gu et al., 2003). It includes the "energy" functionals that are positive definite, and decrease along the trajectories of the system. The Lyapunov-Krasovskii theorem is stated below:

**Lemma 1** (Lyapunov-Krasovskii Stability Theorem) (Gu and Liu, 2009). *Given system (1), suppose that  $f$  maps  $\mathbb{R} \times (\text{bounded sets in } \mathbb{R}^n \times \mathcal{C})$  into bounded sets in  $\mathbb{R}^n$ , and that  $u, v, w : \mathbb{R}_+ \rightarrow \mathbb{R}_+$  are continuous nondecreasing functions, where additionally  $u(s)$  and  $v(s)$  are positive for  $s > 0$ , and  $u(0) = v(0) = 0$ . If there exists a functional  $V : \mathbb{R} \times \mathbb{R}^n \times \mathcal{C} \rightarrow \mathbb{R}$  such that*

$$\begin{cases} u(|\phi(0)|) \leq V(t, \phi) \leq v(|\phi|_h) \\ \dot{V}(t, \phi) \leq -w(|\phi(0)|) \end{cases} \quad (2)$$

*Then the trivial solution of the system (1) is uniformly stable. If  $w(s) > 0$  for  $s > 0$ , then it is uniformly asymptotically stable. If, in addition,  $\lim_{s \rightarrow \infty} u(s) = +\infty$ , then it is globally uniformly asymptotically stable. Such a functional  $V$  is called a Lyapunov-Krasovskii functional (LKF).*

**Definition 2** (Legendre polynomials). *The Legendre polynomials considered over the interval  $[-h, 0]$  are defined by:*

$$\mathcal{L}_k(u) = (-1)^k \sum_{l=0}^K p_l^k \left( \frac{u+h}{h} \right)^l, \quad \forall k \in \mathbb{N} \quad (3)$$

where  $p_l^k = (-1)^l \binom{k}{l} \binom{k+l}{l}$ .

These Legendre polynomials satisfy the following properties:

**Property 3** P3.1 Orthogonality:

$$\int_{-h}^0 \mathcal{L}_k(u) \mathcal{L}_l(u) du = \begin{cases} 0, & k \neq l \\ \frac{h}{2k+1}, & k = l \end{cases} \quad \forall (k, l) \in \mathbb{N}^2 \quad (4)$$

P3.2 Boundary conditions:

$$\begin{cases} \mathcal{L}_k(0) = 1, \\ \mathcal{L}_k(-h) = (-1)^k, \end{cases} \quad \forall k \in \mathbb{N}, \quad (5)$$

P3.3 Differentiation:

$$\dot{\mathcal{L}}_k(u) = \begin{cases} 0, & k = 0 \\ \sum_{i=0}^{k-1} \frac{(2i+1)}{h} (1 - (-1)^{k+i}) \mathcal{L}_i(u), & k \geq 1 \end{cases} \quad (6)$$

We remark that the set of Legendre polynomials  $\{\mathcal{L}_k, k \in \mathbb{N}\}$  forms an orthogonal sequence according to the P3.1 Orthogonality.

**Definition 4** (Bessel inequality). Given  $\{\mathcal{L}_k, k \in \mathbb{N}\}$  be an orthogonal sequence, for any scalar function  $\phi : [-h, 0] \rightarrow \mathbb{R}$ , the following inequality holds:

$$\langle \phi, \phi \rangle \geq \sum_{k=0}^N \frac{\langle \phi, \mathcal{L}_k \rangle^2}{\langle \mathcal{L}_k, \mathcal{L}_k \rangle} \quad (7)$$

**Lemma 5** (Bessel-Legendre inequalities) (Lee et al., 2018). Assuming  $x \in C$ ,  $R \in \mathbb{S}_n^+$ , and  $h > 0$ , the following inequality holds:

$$\int_{-h}^0 x^T(u) Rx(u) du \geq \frac{1}{h} \begin{bmatrix} \Omega_0(x) \\ \Omega_1(x) \\ \vdots \\ \Omega_N(x) \end{bmatrix}^T R_N \begin{bmatrix} \Omega_0(x) \\ \Omega_1(x) \\ \vdots \\ \Omega_N(x) \end{bmatrix} \quad (8)$$

where  $\Omega_k(x) = \int_{-h}^0 \mathcal{L}_k(u) x(u) du$ ,  $k = 0, \dots, N$  and  $R_N = \text{diag}\{R, 3R, \dots, (2N+1)R\}$ .

**Proof** See Appendix A for detailed proof.

**Remark 6** Special cases of  $N = 0$  and  $N = 1$  in Bessel-Legendre inequalities can lead to Jensen's Inequality and the Wirtinger-based integral inequality (Seuret and Gouaisbaut, 2013), and the auxiliary function-based integral inequality (Park et al., 2015).

**Remark 7** The set of orthogonal sequences  $\{\mathcal{L}_k, k \in \mathbb{N}\}$  represents a basis of  $C([-h, 0], \mathbb{R}^n)$  since it is dense in  $C([-h, 0], \mathbb{R}^n)$ . Furthermore, the Bessel-Legendre inequality tends to equality if  $N \rightarrow \infty$ :

$$\int_{-h}^0 x^T(u) Rx(u) du = \frac{1}{h} \begin{bmatrix} \Omega_0(x) \\ \Omega_1(x) \\ \vdots \\ \Omega_N(x) \end{bmatrix}^T R_N \begin{bmatrix} \Omega_0(x) \\ \Omega_1(x) \\ \vdots \\ \Omega_N(x) \end{bmatrix} \quad (9)$$

### 3. Problem statement

Consider a group of  $n$  AVs moving along a single lane and forming a CAV platoon. Fig. 1 shows the schematic of the CAV platoon, where the dashed line denotes that there is communication between the two CAVs. It is worth mentioning that each CAV communicates with arbitrarily other CAVs in the platoon for the sake of generalization in the schematic. Nevertheless, the communication digraph is different in practice, depending on the different IFTs adopted. Via intra-vehicle communication (e.g., C-V2X according to the meeting report from Federal Communications Commission (Verizon North, 2020)), all vehicles share their state information (e.g., the absolute position, velocity, and acceleration)



**Figure 1:** The schematic of the CAV platoon.

with other vehicles within the platoon according to the IFT. It is assumed that each CAV is equipped with i) an on-board radar responsible for collision detection via measuring the gap distance between any two consecutive vehicles, ii) a built-in GPS sensor for measuring the longitudinal position, iii) a wireless on-board unit for communicating potentially useful information with its proximal vehicles via the C-V2X communication, iv) an upper-level controller for calculating the desired longitudinal acceleration based on the parameters obtained, and v) a lower-level controller for determining the throttle and brake actuator inputs to track the desired acceleration. Such an assumption is reasonable as the sensing, communication, and actuation units requested above are available in modern CAVs, and thus do not require specific changes in the existing vehicle configuration. Note that the on-board radar only functions when communication is unavailable or malfunctioning since more accurate information can be obtained via communication in a more efficient manner.

### 3.1. Vehicle longitudinal dynamic Modeling

Let  $p_i(t)$ ,  $v_i(t) = \dot{p}_i(t)$ ,  $a_i(t) = \ddot{p}_i(t)$ , and  $\dot{a}_i(t) = \ddot{\ddot{p}}_i(t) \in \mathbb{R}$  denote the longitudinal position, speed, acceleration, and jerk of vehicle  $i$  at time  $t$ , respectively. A vehicle longitudinal dynamic model mainly consists of the engine, throttle and brake actuators, drive train, transmission, and torque converter. Under a variety of resistance forces, the longitudinal dynamics of vehicle  $i$  can be modeled by the following force balance equation:

$$m_i a_i(t) = f_i^e(t) - f_i^g(t) - f_i^w(t) - f_i^r(t) \quad (10)$$

where  $m_i$  stands for the unknown mass of vehicle  $i$ ;  $f_i^e(t)$  is the desired engine force acting on vehicle  $i$ ;  $f_i^g(t)$ ,  $f_i^w(t)$ , and  $f_i^r(t)$  denote the gravity component parallel to the road surface, air resistance force, and rolling resistance force, respectively.

However, Equation (10) is nonlinear, which brings difficulty to the design of its controller. Hence a feedback control in Appendix B is employed to transfer Equation (10) into the linear form:

$$\tau_i \dot{a}_i(t) + a_i(t) = u_i(t) \quad (11)$$

where  $u_i(t)$  denotes the control input of the lower-level controller, which can be interpreted as the desired acceleration of vehicle  $i$ ,  $\tau_i$  is the time constant representing the engine actuator delay.

Reformulate Equation (11), the state space equation can be represented as:

$$\dot{x}_i(t) = Ax_i(t) + Bu_i(t) \quad (12)$$

$$\text{with } A = \begin{bmatrix} 0 & 1 & 0 \\ 0 & 0 & 1 \\ 0 & 0 & -\frac{1}{\tau_i} \end{bmatrix} \text{ and } B = \begin{bmatrix} 0 \\ 0 \\ \frac{1}{\tau_i} \end{bmatrix}$$

where  $x_i(t) = [p_i(t) \ v_i(t) \ a_i(t)]^T \in \mathbb{R}^3$  denotes the state vector of vehicle  $i$ .

As for the reference leading dynamics, it can be described as (Hengster-Movric et al., 2015):

$$\dot{x}_1(t) = Ax_1(t) \quad (13)$$

where  $x_1(t) = [p_1(t) \ v_1(t) \ a_1(t)]^T \in \mathbb{R}^3$ .

As for the control strategy, due to the presence of limited communication, the control input of the vehicle  $i$  is determined by an appropriate decentralized coupling protocol of communication information:

$$u_i = u_i \underbrace{\left( x_1(t-h), \dots, x_i(t-h), \dots, x_n(t-h) \right)}_n \quad (14)$$

where  $h$  represents the communication delay within the transmission range which is assumed to be similar among different IFTs (Zheng et al., 2015; Vukadinovic et al., 2018; Vu et al., 2020; Martín-Sacristán et al., 2020; Pirani et al., 2022).

Here we assume that CAVs adopt the Constant Distance (CD) policy and Leader-based IFT in which CAVs maintain a desired distance from the reference leader. Then the cooperative leader tracking problem can be formulated as follows:

$$\begin{cases} \lim_{t \rightarrow \infty} \|p_i(t) - p_1(t) - d_{i1}\| = 0 \\ \lim_{t \rightarrow \infty} \|v_i(t) - v_1(t)\| = 0 \quad \forall i = 1, \dots, N \\ \lim_{t \rightarrow \infty} \|a_i(t) - a_1(t)\| = 0 \end{cases} \quad (15)$$

where  $d_{i1}$  denotes the desired intra-vehicle distance of vehicle  $i$  from the leading vehicle.

The consensus goal (15) can be achieved using an appropriate distributed strategy. Therefore, the vehicle  $i$  adjusts its dynamics through the following decentralized coupling protocol computed onboard as:

$$u_i = - \sum_{j=1}^n a_{ij} k_{ij}^T [ p_i(t-h) - p_j(t-h) - d_{ij} \quad v_i(t-h) - v_j(t-h) \quad a_i(t-h) - a_j(t-h) ]^T \quad (16)$$

where

$a_{ij}$  denotes the weight of the edge  $(i, j)$ , and  $a_{ij} = 0$  if there is no edge  $(i, j)$ ;

$d_{ij}$  stands for the desired intra-vehicle distance of vehicle  $i$  from the vehicle  $j$ ;

$k_{ij} = [ \alpha_{ij} \quad \beta_{ij} \quad \gamma_{ij} ]^T \in \mathbb{R}^3$  presents the feedback control gain vector;

$\alpha_{ij}$ ,  $\beta_{ij}$ , and  $\gamma_{ij}$  denote the control gain of spacing error, speed error, and acceleration error, respectively.

### 3.2. Closed-loop Vehicle Network Modeling

To prove the consensus of systems (12) and (13) under the action of coupling protocol (16), we define the error state with respect to the leader as:

$$e_i(t) = \begin{bmatrix} \tilde{p}_i \\ \tilde{v}_i \\ \tilde{a}_i \end{bmatrix} = \begin{bmatrix} p_i - p_1 - d_{i1} \\ v_i - v_1 \\ a_i - a_1 \end{bmatrix} \quad (17)$$

Then the decentralized coupling protocol (16) can be reformulated as:

$$u_i = - \sum_{j=1}^n a_{ij} k_{ij}^T [ e_i(t-h) - e_j(t-h) ] \quad (18)$$

Therefore, the dynamics of the error system can be presented as:

$$\begin{cases} \dot{\tilde{p}}_i = \tilde{v}_i \\ \dot{\tilde{v}}_i = \tilde{a}_i \\ \dot{\tilde{a}}_i = -\frac{1}{\tau} \tilde{a}_i - \frac{1}{\tau} \sum_{j=0}^n a_{ij} k_{ij}^T (e_i(t-h) - e_j(t-h)) \end{cases} \quad (19)$$

From Equation (19), the dynamics of the closed-loop vehicular network can be recast in a compact form as:

$$\dot{e}_i(t) = A e_i(t) - B \sum_{j=0}^n a_{ij} k_{ij}^T (e_i(t-h) - e_j(t-h)) \quad (20)$$

**Theorem 8** The closed-loop network system adopting constant communication delay, Leader-based IFT, and CD policy can be presented as a linear state delay system:

$$\begin{cases} \dot{X}(t) = A^* X(t) + \Psi X(t-h), & \forall t \geq 0 \\ X(t) = \phi(t), & \forall t \in [-h, 0] \end{cases} \quad (21)$$

with

$$\left\{ \begin{array}{l} A^* = I_n \otimes A \in \mathbb{R}^{3n \times 3n} \\ \Psi = -B^* \mathcal{F} (E_1 - E_2) \in \mathbb{R}^{3n \times 3n} \\ B^* = I_n \otimes B \in \mathbb{R}^{3n \times n} \\ \mathcal{K} = [k_{ij}]_{n \times n} \\ \mathcal{H} = \mathcal{A}^\circ \mathcal{K} = [a_{ij} \otimes k_{ij}^T]_{N \times N} \in \mathbb{R}^{n \times 3n} \\ \mathcal{F} = \text{diag} \left\{ \underbrace{\mathcal{H}_1, \mathcal{H}_2, \dots, \mathcal{H}_N}_{n} \right\} \in \mathbb{R}^{n \times 3n^2} \\ \mathcal{H}_i = \underbrace{[a_{i1} k_{i1}^T, a_{i2} k_{i2}^T, \dots, a_{in} k_{in}^T]}_n \in \mathbb{R}^{1 \times 3n} \forall i \in \mathcal{V} \\ E_1 = \text{diag} \left\{ \underbrace{I_1, I_1, \dots, I_1}_n \right\} \in \mathbb{R}^{3n^2 \times 3n} \\ E_2 = \left[ \underbrace{I_2^T, \dots, I_2^T}_n \right]^T \in \mathbb{R}^{3n^2 \times 3n} \\ I_1 = \left[ \underbrace{I_3^T, \dots, I_3^T}_n \right]^T \in \mathbb{R}^{3n \times 3} \\ I_2 = I_{3n} \in \mathbb{R}^{3n \times 3n} \\ I_3 = I_3 \in \mathbb{R}^{3 \times 3} \end{array} \right.$$

where  $X(t) = [e_1^T \ \dots \ e_n^T]^T \in \mathbb{R}^{3n}$  stands for the error state vector of the closed-loop vehicular network;  $\phi$  is the initial conditions;  $A^*$  and  $\Psi$  are constant matrix according to their definitions.

**Proof** Theorem 8 can be obtained by manipulating matrix transformations on the error state vector of the closed-loop vehicular network and Equation (20).

#### 4. Stability analyses

The primary idea of Lemma 1 is to determine a positive definite functional whose derivative with respect to time along the trajectories of the system (21) is negative definite. Therefore, the local stability of the closed-loop network system (21) can be guaranteed by proposing a candidate LKF  $V$  and providing some conditions that guarantee its positive definiteness and the negative definiteness of its derivative. In the stability analysis of such systems using LKF, several types of functionals have been provided in the literature. Among them, an integral quadratic term is one of the most relevant components (Fridman et al., 2003):

$$V(X_t) = \int_{-h}^0 \int_u^0 \dot{X}_t^T(\theta) R \dot{X}_t(\theta) d\theta du \quad (22)$$

Differentiating Equation (22) with respect to  $t$  leads to:

$$\dot{V}(X_t) = h \dot{X}_t^T(t) R \dot{X}_t(t) - \int_{-h}^0 \dot{X}_t^T(u) R \dot{X}_t(u) du \quad (23)$$

In order to transform Equation (23) into a suitable LMI setup, an over-approximate process of the integral terms is adopted since it cannot be straightforwardly converted in the quadratic formulation described above.

Thanks to Lemma 5, the lower bound of  $\int_{-h}^0 \dot{X}_t^T(u) R \dot{X}_t(u) du$  can be derived by the following Corollary:

**Corollary 9** Let  $\dot{x}$  be such that  $\dot{x} \in C$ ,  $R \in \mathbb{S}_n^+$ , and  $h > 0$ . Then, the integral inequality

$$\int_{-h}^0 \dot{x}^T(u) R \dot{x}(u) du \geq \frac{1}{h} \xi_N^T \left[ \sum_{k=0}^N (2k+1) \Gamma_N(k)^T R \Gamma_N(k) \right] \xi_N, \quad (24)$$

holds for all integers  $N \in \mathbb{N}$  where

$$\xi_N = \begin{cases} \begin{bmatrix} x^T(0) & x^T(-h) \end{bmatrix}^T, & \text{if } N = 0, \\ \begin{bmatrix} x^T(0) & x^T(-h) & \frac{1}{h} \Omega_0^T & \cdots & \frac{1}{h} \Omega_{N-1}^T \end{bmatrix}^T, & \text{if } N > 0, \end{cases} \quad (25)$$

**Proof** See Appendix C for detailed proof.

Define the lower bound by Corollary 9, and the stability theorem with an arbitrary  $N$  follows.

**Theorem 10** For a given integer  $N$  and a constant delay  $h$ , assume that there exists a matrix  $P_N \in \mathbb{S}_{(N+1)n}$  and two matrices  $S, R \in \mathbb{S}_n^+$  such that the LMIs

$$\begin{aligned} \Theta_N(h) &= \begin{cases} P_N > 0, & \text{if } N = 0 \\ P_N + \frac{1}{h} \text{diag}(0_{nn}, S_{N-1}) > 0, & \text{if } N > 0 \end{cases} \\ \Phi_N(h) &= \Phi_{N0}(h) - \begin{bmatrix} \Gamma_N(0) \\ \vdots \\ \Gamma_N(N) \end{bmatrix}^T R_N \begin{bmatrix} \Gamma_N(0) \\ \vdots \\ \Gamma_N(N) \end{bmatrix} < 0 \end{aligned} \quad (26)$$

hold, where

$$\begin{cases} \Phi_{N0}(h) = \text{He}(G_N^T(h) P_N H_N) + \tilde{S}_N + h^2 F_N^T R F_N, \\ \tilde{S}_N = \text{diag}\{S, -S, 0_{Nn}\}, \\ S_N = \text{diag}\{S, 3S, \dots, (2N+1)S\}, \\ F_N = [A^* \quad \Psi \quad 0_{n,nN}], \\ G_N(h) = \begin{bmatrix} I & 0_n & 0_{n,nN} \\ 0_{nN,n} & 0_{nN,n} & hI_{nN} \end{bmatrix}, \\ H_N = [F_N^T \quad \Gamma_N^T(0) \quad \Gamma_N^T(1) \dots \Gamma_N^T(N-1)]^T. \end{cases} \quad (27)$$

Then system (21) is asymptotically stable for the constant delay  $h$ .

**Proof** See Appendix D for detailed proof.

**Remark 11** Taking  $N = 0$  in Theorem 10 allows retrieving one of the most classical delay-dependent stability conditions based on Jensen's inequality and LMI (Gouaisbaut and Peaucelle, 2006). Additionally, choosing  $N = 1$  leads to the stability conditions from Seuret and Gouaisbaut (2013).

## 5. Numerical analyses

### 5.1. Network and traffic scenario

#### 5.1.1. Simulation setting

To validate the theoretical results, we refer to a platoon consisting of five CAVs (as depicted in Fig. 1) on a single-lane highway as a representative example. According to the definition of Leader-based IFTs, the leader communicates with all vehicles by broadcasting its information while other vehicles only communicate with their neighbors according to the IFT adopted. Here, we take the four most widely adopted Leader-based IFTs (Leader-Follower (LF), Leader-Predecessor-Follower (LPF), Leader-Multiple-predecessors-Follower (LMPF), and Leader-Bi-Direction (LBD)) as an

**Table 1**  
Network and traffic simulation parameters.

Parameters	Value
Platoon size $n$	5 vehicles
Vehicle length $L$	5 [m]
Engine actuator delay $\tau_i$	0.2 [s] <sup>1</sup>
Communication delay $h$	0.3 [s] <sup>2</sup>
Weight of edge $(i, j)$ $a_{ij}$	$\frac{1}{d_i}$
Feedback control gain vector $k_{ij}$	$\begin{cases} [0.2, 0.4, 0.2]^T & \text{for } i = 2; \\ [0.3, 0.3, 0.2]^T & \text{for } i = 3; \\ [0.3, 0.4, 0.3]^T & \text{for } i = 4; \\ [0.3, 0.4, 0.2]^T & \text{for } i = 5. \end{cases}$
Desired intra-vehicle distance $d_{ij}$	15 [m]

<sup>1</sup> (Wang et al., 2018; Zhou et al., 2020)

<sup>2</sup> (Abbas et al., 2018; Thota et al., 2019)

example to analyze tracking performance and safety. The caveat is that although parameters should be selected based on the specific control structure in practical. In order to obtain a simulation result for further analysis, the parameters for both network and traffic simulation are reported in Table 1 for simplicity but without loss of generality. Note that the weighted adjacent matrix is set to  $a_{ij} = \frac{1}{d_i}, \forall (i, j) \in \mathcal{E}$  denote that all the information of neighbors is playing an equal role in control decisions. Moreover, different CAV set different control gains to simulate heterogeneity.

### 5.1.2. Introduction to the common Leader-based IFTs

In this section, we give a detailed introduction to the four most widely adopted Leaders-based IFTs (LF, LPF, LMPF, and LBD) and the corresponding derivation of the dynamic equation. The communication schematic of the typical four Leader-based IFTs is shown in Fig. 2, where dotted lines with an arrow denote the one-direction communication while dotted lines without arrows represent the bi-direction communication.

#### The case of LF

For LF, all CAVs in the platoon only obtain information from the leader. The Equation (18) can be reformed as follows:

$$u_i(t) = a_{i1} k_{i1}^T [e_i(t-h) - e_1(t-h)] \quad (28)$$

Substitute Equation (28) into Equation (11), the dynamic equation of LF can be obtained as:

$$\begin{aligned} \dot{a}_i(t) &= -\frac{1}{\tau_i} a_{i1} [\alpha_{i1} (\tilde{p}_i(t-h) - \tilde{p}_1(t-h)) + \beta_{i1} (\tilde{v}_i(t-h) - \tilde{v}_1(t-h)) + \gamma_{i1} (\tilde{a}_i(t-h) - \tilde{a}_1(t-h))] - \frac{1}{\tau_i} a_i(t) \\ &= -\frac{1}{\tau_i} a_{i1} [\alpha_{i1} \tilde{p}_i(t-h) + \beta_{i1} \tilde{v}_i(t-h) + \gamma_{i1} \tilde{a}_i(t-h)] - \frac{1}{\tau_i} a_i(t) \\ &= -\frac{1}{\tau_i} a_{i1} [\alpha_{i1} (p_i(t-h) - p_1(t-h) - d_{i1}) + \beta_{i1} (v_i(t-h) - v_1(t-h)) + \gamma_{i1} (a_i(t-h) - a_1(t-h))] - \frac{1}{\tau_i} a_i(t) \end{aligned} \quad (29)$$

#### The case of LPF

As for LPF, all CAVs in the platoon obtain information from both the leader and the immediate predecessor. The decentralized coupling protocol (18) can be reformed as follows:

$$u_i = -a_{i1} k_{i1}^T [e_i(t-h) - e_1(t-h)] - a_{i(i-1)} k_{i(i-1)}^T [e_i(t-h) - e_{i-1}(t-h)] \quad (30)$$

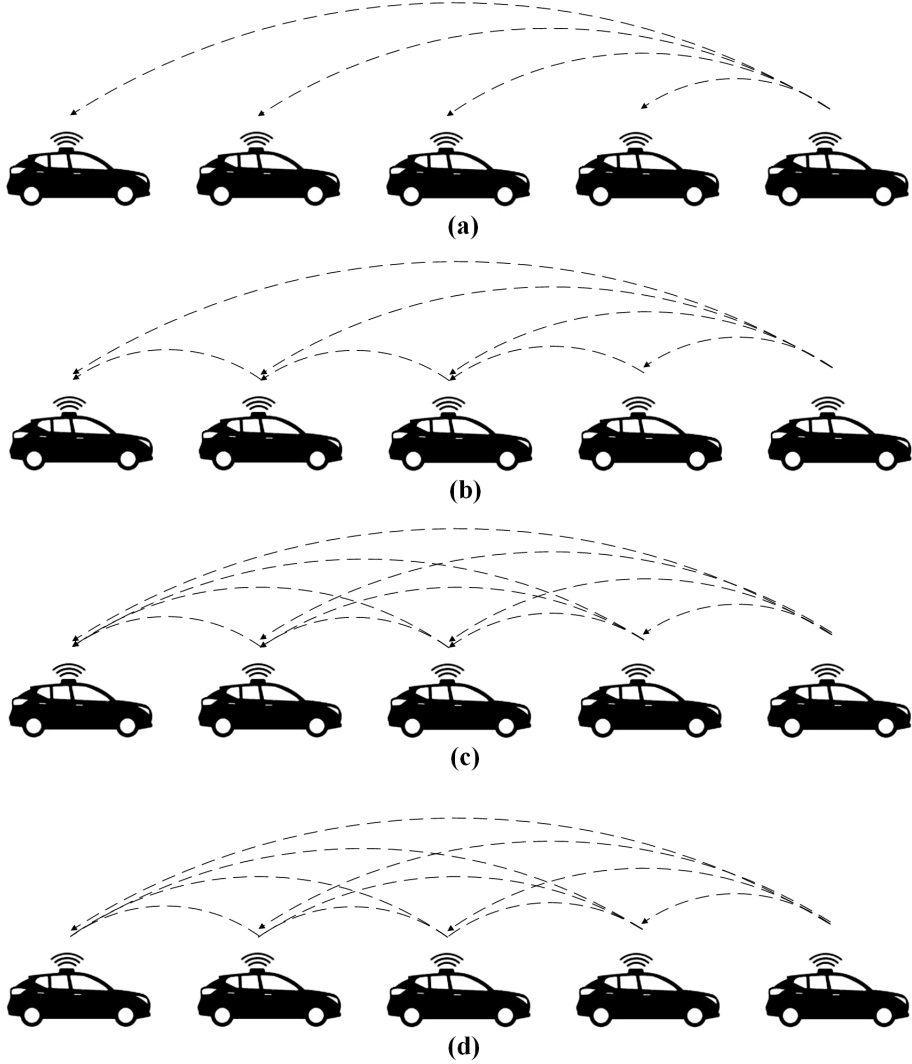


**Figure 2:** The communication schematic of typical three Leader-based IFTs for the CAV platoon: (a) Leader-Follower (LF); (b) Leader-Predecessor-Follower (LPF); (c) Leader-Multiple-predecessors-Follower (LMPF); and (d) Leader-Bi-Direction (LBD), where dotted lines with an arrow denote the one-direction communication while dotted lines without arrows represent the bi-direction communication.

Then, the dynamic equation of LPF can be obtained as:

$$\begin{aligned}
 \dot{a}_i(t) = & -\frac{1}{\tau_i} a_i(t) - \frac{1}{\tau_i} [a_{i1} [\alpha_{i1} (\tilde{p}_i(t-h) - \tilde{p}_1(t-h)) + \beta_{i1} (\tilde{v}_i(t-h) - \tilde{v}_1(t-h)) + \gamma_{i1} (\tilde{a}_i(t-h) - \tilde{a}_1(t-h))] \\
 & + a_{i(i-1)} [\alpha_{i(i-1)} (\tilde{p}_i(t-h) - \tilde{p}_{i-1}(t-h)) + \beta_{i(i-1)} (\tilde{v}_i(t-h) - \tilde{v}_{i-1}(t-h)) \\
 & + \gamma_{i(i-1)} (\tilde{a}_i(t-h) - \tilde{a}_{i-1}(t-h))] \\
 = & -\frac{1}{\tau_i} a_i(t) - \frac{1}{\tau_i} [a_{i1} [\alpha_{i1} (p_i(t-h) - p_1(t-h) - d_{i1}) + \beta_{i1} (v_i(t-h) - v_1(t-h)) + \gamma_{i1} (a_i(t-h) - a_1(t-h))] \\
 & + a_{i(i-1)} [\alpha_{i(i-1)} (p_i(t-h) - p_{i-1}(t-h) - d_{i(i-1)}) + \beta_{i(i-1)} (v_i(t-h) - v_{i-1}(t-h)) \\
 & + \gamma_{i(i-1)} (a_i(t-h) - a_{i-1}(t-h))]
 \end{aligned} \tag{31}$$

### The case of LMPF

In addition, for LMPF, all CAVs in the platoon are able to obtain information from the leader and all predecessors. The decentralized coupling protocol (18) can be reformed as follow:

$$u_i = - \sum_{j=1}^{i-1} a_{ij} k_{ij}^T [e_i(t-h) - e_j(t-h)] \quad (32)$$

The dynamic equation of LMPF can be presented as:

$$\begin{aligned} \dot{a}_i(t) &= -\frac{1}{\tau_i} a_i(t) \\ &\quad - \frac{1}{\tau_i} \sum_{j=1}^{i-1} a_{ij} [\alpha_{ij}(\tilde{p}_i(t-h) - \tilde{p}_j(t-h)) + \beta_{ij}(\tilde{v}_i(t-h) - \tilde{v}_j(t-h)) + \gamma_{ij}(\tilde{a}_i(t-h) - \tilde{a}_j(t-h))] \\ &= -\frac{1}{\tau_i} a_i(t) \\ &\quad - \frac{1}{\tau_i} \sum_{j=1}^{i-1} a_{ij} [\alpha_{ij} (p_i(t-h) - p_j(t-h) - d_{ij}) + \beta_{ij} (v_i(t-h) - v_j(t-h)) + \gamma_{ij} (a_i(t-h) - a_j(t-h))] \end{aligned} \quad (33)$$

### The case of LBD

For LBD, all CAVs in the platoon except the leader are able to obtain information from each vehicle. The decentralized coupling protocol can still be represented by Equation (18). The dynamic equation of LBD can be presented as:

$$\begin{aligned} \dot{a}_i(t) &= -\frac{1}{\tau_i} a_i(t) \\ &\quad - \frac{1}{\tau_i} \sum_{j=1}^n a_{ij} [\alpha_{ij}(\tilde{p}_i(t-h) - \tilde{p}_j(t-h)) + \beta_{ij}(\tilde{v}_i(t-h) - \tilde{v}_j(t-h)) + \gamma_{ij}(\tilde{a}_i(t-h) - \tilde{a}_j(t-h))] \\ &= -\frac{1}{\tau_i} a_i(t) \\ &\quad - \frac{1}{\tau_i} \sum_{j=1}^n a_{ij} [\alpha_{ij} (p_i(t-h) - p_j(t-h) - d_{ij}) + \beta_{ij} (v_i(t-h) - v_j(t-h)) + \gamma_{ij} (a_i(t-h) - a_j(t-h))] \end{aligned} \quad (34)$$

## 5.2. Tracking performance of Leader-based IFTs

Firstly, in the preliminary analysis, we start considering the tracking performance of the four IFTs studied. From this perspective, the tracking performances have been evaluated considering two representative leader maneuvers, namely:

1. **Trapezoidal signal:** The leader suddenly decelerates to 14.6m/s at  $-0.15m/s^2$  and keeps it for 36s. Then the leader accelerates back to 20m/s at  $0.3m/s^2$  (see Fig. 3(a, b)).
2. **Oscillation signal:** The leader suddenly accelerates to 23.6m/s in 12s and keeps the velocity for 15s. Then the leader decelerates to 16.4m/s in 12s and accelerates back to 20m/s in 12s (see Fig. 3(c, d)).

Once the platoon is formed and all CAVs reach the equilibrium state where the tracking error is 0, we adopt the trapezoidal signal in Fig. 3(a, b) as the leader maneuver to test the tracking performance of the four IFTs. Results in Fig. 4 confirm the theoretical analysis and show how CAVs track the lead. As expected, all CAVs in the platoon enable fast and smooth tracking of the motion of the leader. Besides, transient changes in the reference signal arise abrupt changes in the tracking error. Nevertheless, such errors are diminished over time thanks to the stability property. In addition, the tracking speed and overshoot of different CAV amounts for transient responses to changes in the reference signal are different due to different control gains adopted.

Besides, the tracking performance of the four IFTs has also been tested here for the oscillation signal defined in Fig. 3(c, d). In this case, Fig. 5 shows the tracking performance of the four IFTs. It demonstrates excellent cooperative

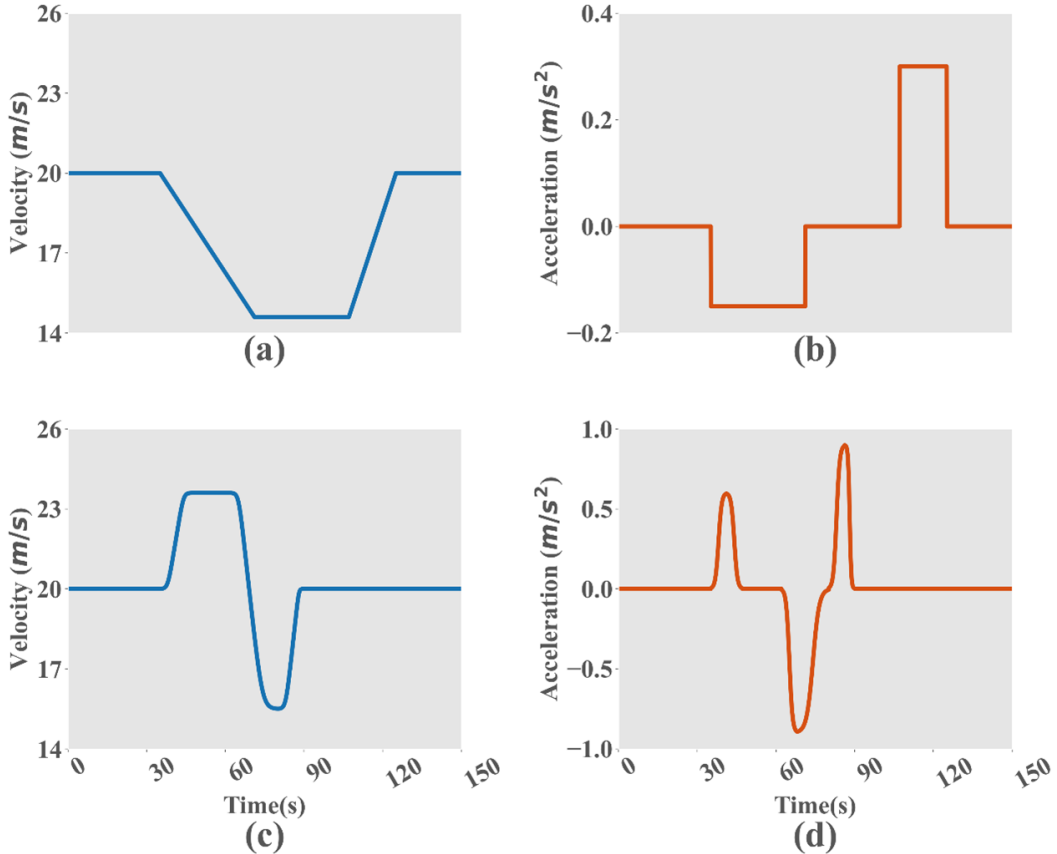


**Figure 3:** The two representative leader maneuvers: (a) and (b) denote the velocity and acceleration of the trapezoidal signal, respectively; (c) and (d) denote the velocity and acceleration of the oscillation signal, respectively.

tracking behavior since each CAV can track the reference signal steadily while maintaining the rigid formation requirements. Moreover, the tracking error is caused by transient changes in the reference signal and decays smoothly over time, as in the case of the trapezoidal signal. Furthermore, Figs. 4,5 verify the effectiveness of the four IFTs on tracking performance and stability.

### 5.3. Safety analyses considering hard braking maneuver

To further evaluate the safety in all the different driving and communication scenarios, we have also quantitatively analyzed the possible emergence of critical driving situations for all IFTs under investigation by exploiting the safety indicator Deceleration Rate to Avoid the Crash (DRAC), which is well known in the literature (Saccomanno et al., 2008; Fu and Sayed, 2021). This indicator presents the deceleration rate needed to be applied by a vehicle to avoid a collision with another vehicle which can be defined for each vehicle  $i$  at the time  $t$  as follows:

$$DRAC_i(t) = \frac{(v_i(t) - v_{i-1}(t))^2}{2(p_{i-1}(t) - p_i(t) - L)} \quad (35)$$

Moreover, we consider here the occurrence of hard braking (emergency) maneuver as an additional evaluation scenario. Specifically, results in Fig. 6 show how the platoon reacts in the case of a braking maneuver performed by the leader for each IFT under investigation. Once again, in this case, all CAVs under each IFT smoothly track the motion of the leader during hard braking avoiding possible collisions. Furthermore, the variation of selected safety indicator DRAC over time under different IFTs is shown in Fig. 7 to explore the changes in the security situation under the hard braking maneuver. It is worth mentioning that the variation of the leader is omitted since it has no predecessor,

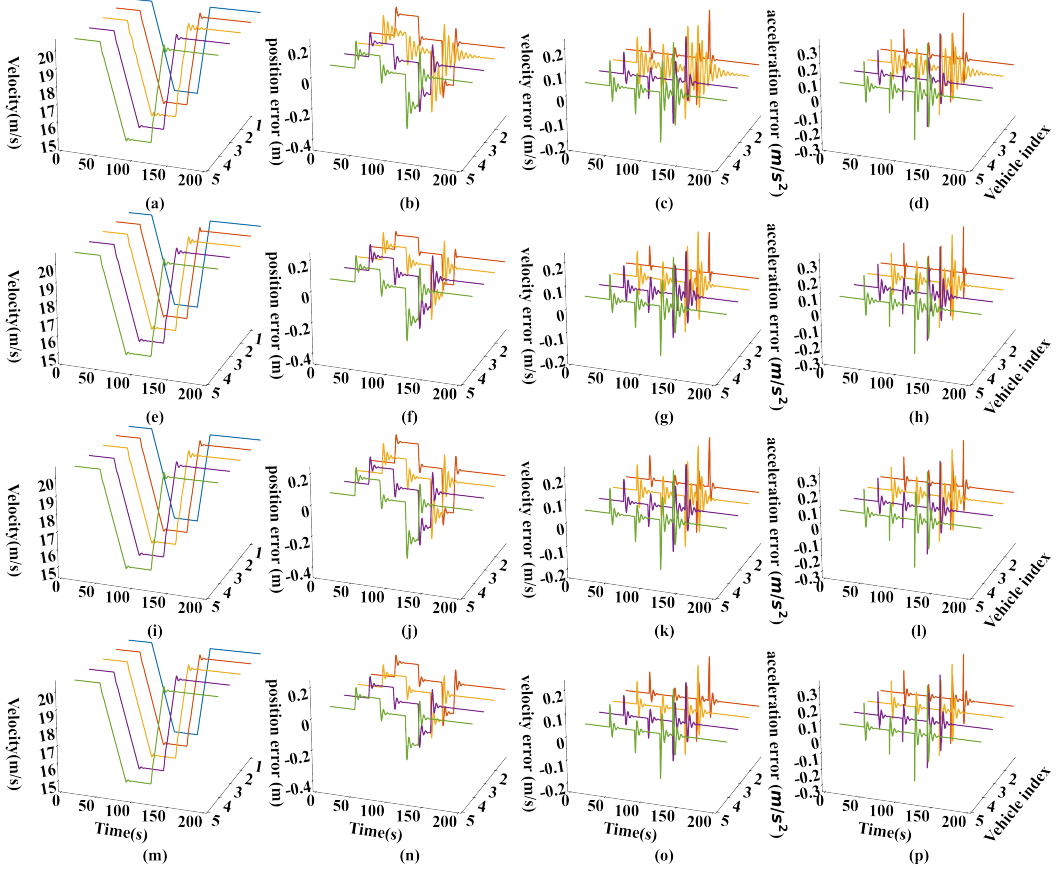


**Figure 4:** Tracking performance for the Trapezoidal signal in Fig. 3(a,b) under the four IFTs: (a), (b), (c), and (d) present tracking results under LF, including the velocity, tracking error of position, tracking error of velocity, and tracking error of acceleration, respectively; (e), (f), (g), and (h) show the case under LPF; (i), (j), (k), and (l) denote the case under LMPF; (m), (n), (o), and (p) show the case under LBD.

which will raise the risk of collisions. Besides, the CAV2, CAV3, CAV4, and CAV5 refer to the second, third, fourth, and fifth CAV in the CAV platoon, respectively.

From Fig. 7, one phenomenon worth pointing out is that the CAV platoon is able to maintain a safety condition under hard braking maneuver. Since DRAC is less than 0.1 all-time, whatever Leader-based IFT and the control gain value under investigation are chosen. Moreover, from a vertical perspective, the case under LBD can provide better safety conditions than the other three one-direction communication IFTs. Besides, from a horizontal point of view, the choice of different control gains can significantly affect the variation of the safety indicator. The control gains of CAV3 are not conducive to safe driving due to its DRAC being significantly higher than other control gain schemes. Furthermore, different IFTs also affect the safety indicator. For example, the DRAC of CAV5 under LF is remarkably higher than that of CAV2 and CAV4. However, it can be kept low under the other three IFTs relative to the case under LF, since it can obtain more information to ensure safe driving. The case of CAV4 is quite the opposite, where the DRAC of CAV4 under LPF is significantly higher than the other three IFTs due to the additional poor information received from the immediate predecessor. In general, bi-direction communication and receiving more information in most cases enable a better safety condition for hard braking maneuver situations.

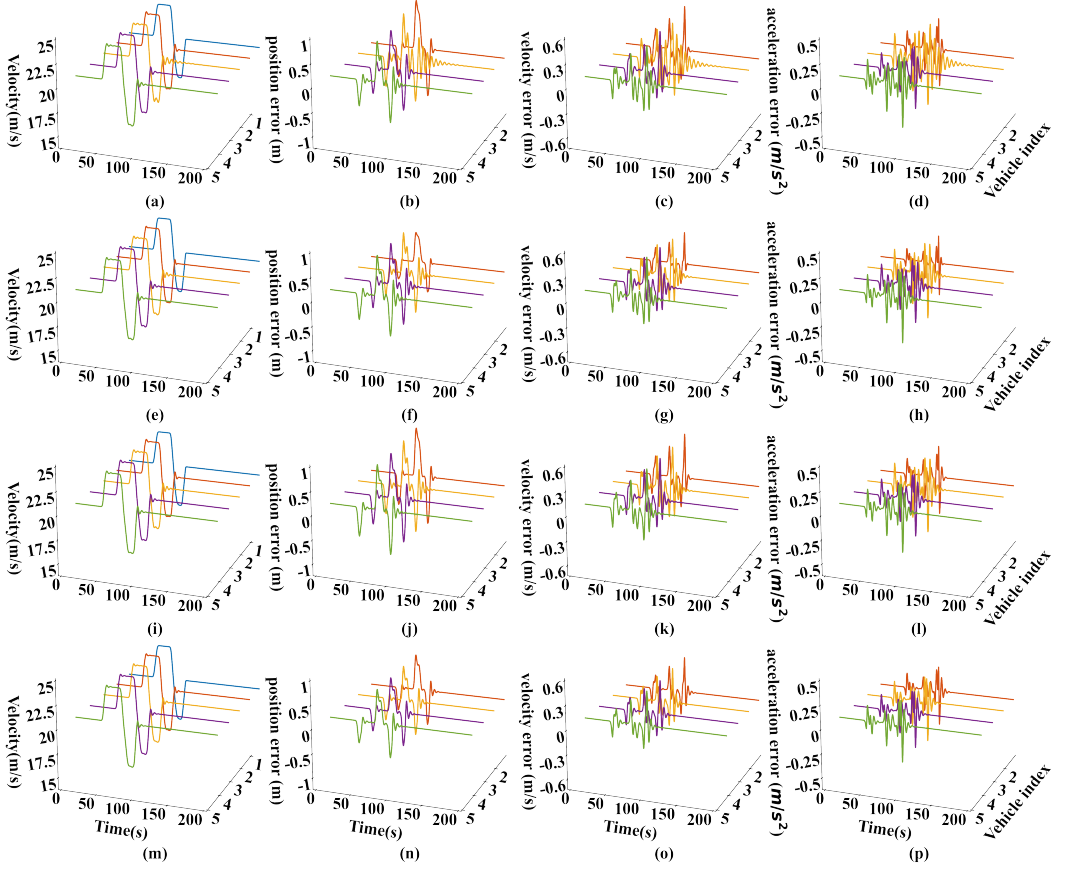


**Figure 5:** Tracking performance for the Oscillation signal in Fig. 3(c,d) under the four IFTs: (a), (b), (c), and (d) present tracking results under LF, including the velocity, tracking error of position, tracking error of velocity, and tracking error of acceleration, respectively; (e), (f), (g), and (h) show the case under LPF; (i), (j), (k), and (l) denote the case under LMPF; (m), (n), (o), and (p) show the case under LBD.

## 6. Conclusion and future work

This paper proposed a general representation of the heterogeneous CAV platoon under the Leader-based IFT considering communication delay and engine actuator delay. To develop this general representation, graph theory was applied to depict communication within the CAV platoon under the Leader-based IFT, and a generic state model was established based on the dynamics of the closed-loop vehicular network. In addition, a novel and more unconservative stability condition of the CAV platoon was developed by applying the B-L inequalities and Lyapunov-Krasovskii Stability Theorem based on the general representation. Furthermore, a comprehensive performance evaluation analysis of the four typical Leader-based IFTs was conducted to reveal tracking performance, transient response, and safety conditions in various scenarios. Last but not least, this paper sheds some light on the relationship between safety conditions, control gains, and IFTs.

Admittedly, we acknowledge that the vehicle behavior is a simplified simulation of reality, and further field tests with more realistic vehicle dynamics models are needed. Moreover, this paper only deals with the case that adopts the CD policy while the Constant Time Headway policy is also widely adopted, which needs further investigation. Similarly, a more general IFTs need to be extended in further studies rather than only Leader-based IFTs. Another question to investigate further is that the communication delay adopted in this paper is the upper bound assumed to be constant for simplification. However, the communication delay is time-varying which changes with the surrounding

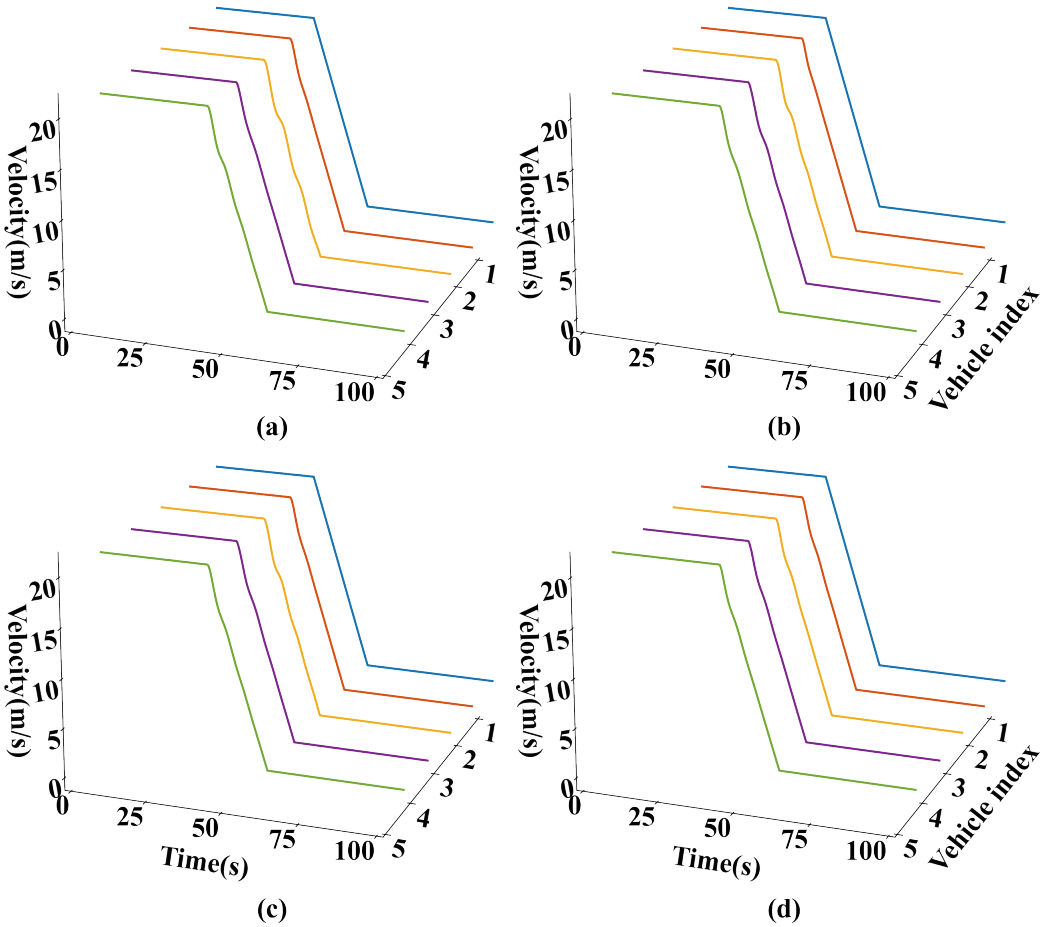


**Figure 6:** Tracking performance for a hard braking maneuver for each IFT under investigation: (a) LF; (b) LPF; (c) LMPF; (d) LBD.

environment. Future research is also needed toward developing a novel stability theorem to deal with time-varying communication delays.

## Appendix A. Proof of Lemma 5

Assume a function  $x \in C$ , a matrix  $R \in \mathbb{S}_n^+$ , and  $h > 0$ . Adopt the approximation error between  $x(u)$  and its projection to the orthogonal sequence set  $\{\mathcal{L}_k, k \in \mathbb{N}\}$  with respect to the inner product, which can be defined by:

$$y_N(u) = x(u) - \sum_{k=0}^N \frac{\int_{-h}^0 \mathcal{L}_k(u)x(u)du}{\int_{-h}^0 \mathcal{L}_k^2(u)du} \mathcal{L}_k(u) = x(u) - \sum_{k=0}^N \frac{2k+1}{h} \Omega_k \mathcal{L}_k(u) \quad (36)$$

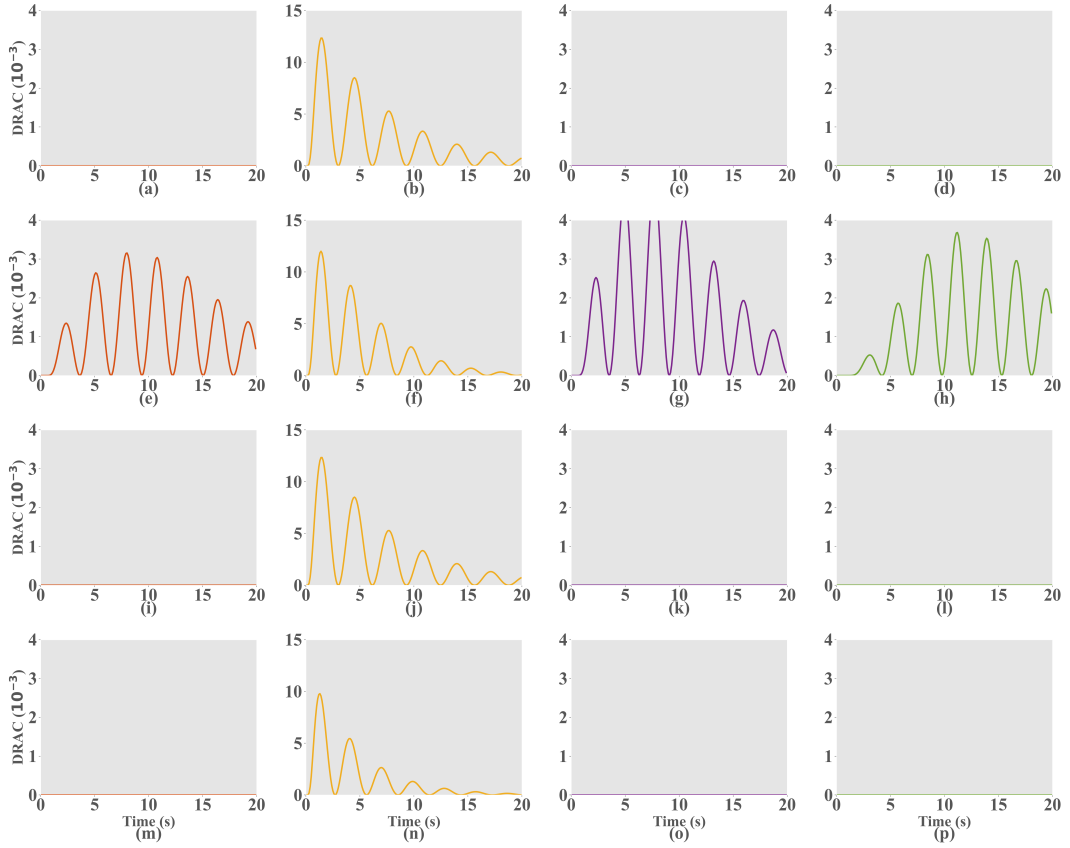


**Figure 7:** The DRAC variation of each CAV for each IFT under investigation: (a), (b), (c), and (d) present DRAC variation under LF of CAV2, CAV3, CAV4, CAV5, respectively; (e), (f), (g), and (h) show the case under LPF; (i), (j), (k), and (l) denote the case under LMPF; (m), (n), (o), and (p) show the case under LBD.

Obviously,  $y_N \in \mathcal{C}$  holds. Moreover, the integral  $\int_{-h}^0 y_N^T(u) R y_N(u) du$  exists and the orthogonal property (4) yields:

$$\begin{aligned} \int_{-h}^0 y_N^T(u) R y_N(u) du &= \int_{-h}^0 x^T(u) R x(u) du \\ &\quad - 2 \sum_{k=0}^N \frac{2k+1}{h} \left( \int_{-h}^0 \mathcal{L}_k(u) x(u) du \right)^T R \Omega_k(x) \\ &\quad + \sum_{k=0}^N \left( \frac{2k+1}{h} \right)^2 \left( \int_{-h}^0 \mathcal{L}_k^2(u) du \right) \Omega_k^T(x) R \Omega_k(x). \end{aligned} \quad (37)$$

According to the definition, some derivation can be provided:

$$\begin{cases} \Omega_k(x) = \int_{-h}^0 \mathcal{L}_k(u) x(u) du \\ \left( \frac{2k+1}{h} \right)^2 \int_{-h}^0 \mathcal{L}_k^2(u) du = \frac{2k+1}{h} \end{cases} \quad (38)$$

Substituting the above Equation into Equation (37), we get:

$$\int_{-h}^0 y_N^T(u) R y_N(u) du = \int_{-h}^0 x^T(u) R x(u) du - \sum_{k=0}^N \frac{2k+1}{h} \Omega_k^T(x) R \Omega_k(x). \quad (39)$$

Moreover, the inequality (8) can be obtained by noting that  $\int_{-h}^0 z_N^\top(u) R z_N(u) du > 0$  for  $R > 0$

## Appendix B. Feedback control for linearization

In this appendix, we provide the linearization of the longitudinal vehicle dynamic in Equation (10). The functions of the lumped uncertain resistance forces, including  $f_i^g(t)$ ,  $f_i^w(t)$ , and  $f_i^r(t)$  are expressed as follows:

$$\begin{cases} f_i^g(t) = m_i g \sin(\theta_i(t)) \\ f_i^w(t) = \frac{1}{2} \rho C_D A_F (v_i(t) + v_w(t))^2 \\ f_i^r(t) = \mu_R m_i g \cos(\theta_i(t)) \end{cases} \quad (40)$$

where  $g = 9.81 \text{m/s}^2$  denotes the acceleration of gravity;  $\theta_i(t)$  is the inclination angle of the road;  $\rho$  denotes the air density;  $C_D$  is the aerodynamic drag coefficient;  $A_F$  represents the maximal cross-sectional/frontal area of the vehicle;  $v_w(t)$  denotes the uncertain headwind speed;  $\mu_R$  is the coefficient of rolling resistance.

The desired engine dynamic is modeled as follows:

$$(\tau_i s + 1) F_i^e = U_i \quad (41)$$

Adopting the inverse Laplace transformation on Equation (41) arrives at:

$$\dot{f}_i^e(t) = \frac{u_i(t)}{\tau_i} - \frac{f_i^e(t)}{\tau_i} \quad (42)$$

Substituting Equation (10) into Equation (42) and differentiating both sides of Equation (42) with respect to time, we get:

$$\begin{aligned} \dot{a}_i(t) &= \frac{\dot{f}_i^e(t)}{m_i} - \frac{\dot{f}_i^g(t)}{m_i} - \frac{\dot{f}_i^{i\omega}(t)}{m_i} - \frac{\dot{f}_i^r(t)}{m_i} \\ &= \frac{u_i(t)}{m_i \tau_i} \\ &\quad - \frac{a_i(t) + g \sin(\theta_i(t)) [1 - \tau_i \mu_R \dot{\theta}_i(t)] + g \cos(\theta_i(t)) [1 + \tau_i \dot{\theta}_i(t)]}{\tau_i} \\ &\quad - \frac{\frac{1}{2} \rho C_D A_F (v_i(t) + v_w(t)) ((v_i(t) + v_w(t)) + 2\tau_i (a_i(t) + \dot{v}_w(t)))}{\tau_i} \end{aligned} \quad (43)$$

Thus, the nonlinear state feedback chosen for linearizing can be defined by:

$$\begin{aligned} u_i^*(t) &= m_i u_i(t) + g \sin(\theta_i(t)) [1 - \tau_i \mu_R \dot{\theta}_i(t)] + g \cos(\theta_i(t)) [1 + \tau_i \dot{\theta}_i(t)] \\ &\quad + \frac{1}{2} \rho C_D A_F (v_i(t) + v_w(t)) ((v_i(t) + v_w(t)) + 2\tau_i (a_i(t) + \dot{v}_w(t))) \end{aligned} \quad (44)$$

Under the new feedback control input, the Equation (10) can be rewritten as:

$$\tau_i \dot{a}_i(t) + a_i(t) = u_i(t) \quad (45)$$

## Appendix C. Proof of Corollary 9

Applying Lemma 5 to the order  $N$ , we get:

$$\int_{-h}^0 \dot{x}^T(u) R \dot{x}(u) du \geq \frac{1}{h} \begin{bmatrix} \Omega_0(\dot{x}) \\ \Omega_1(\dot{x}) \\ \vdots \\ \Omega_N(\dot{x}) \end{bmatrix}^T R_N \begin{bmatrix} \Omega_0(\dot{x}) \\ \Omega_1(\dot{x}) \\ \vdots \\ \Omega_N(\dot{x}) \end{bmatrix} \quad (46)$$

An integration by parts of  $\Omega_k(\dot{x})$  ensures that, for all  $k \geq 0$ :

$$\Omega_k(\dot{x}) = \mathcal{L}_k(0)x(0) - \mathcal{L}_k(-h)x(-h) - \int_{-h}^0 \left( \frac{d}{du} \mathcal{L}_k(u) \right) x(u) du \quad (47)$$

Substituting the Boundary conditions (5) and Differentiation (6) into  $\Omega_k(\dot{x})$ , we get:

$$\Omega_k(\dot{x}) = x(0) - (-1)^k x(-h) + \sum_{i=0}^{k-1} \frac{\gamma_{Nk}^i}{h} \Omega_i(x) = \Gamma_N(k) \xi_N \quad (48)$$

Replacing  $\Omega_k(\dot{x})$  by  $\Gamma_N(k) \xi_N$  leads to Equation (24).

## Appendix D. Proof of Theorem 10

According to the Corollary 9, the states of system need to be extended to  $\tilde{x}_N(t)$  defined as:

$$\tilde{x}_N(t) = \begin{cases} \begin{bmatrix} x_t(0) \\ \int_{-h}^0 \mathcal{L}_0(s)x_t(s)ds \\ \vdots \\ \int_{-h}^0 \mathcal{L}_{N-1}(s)x_t(s)ds \end{bmatrix} & \text{if } N \geq 1, \\ x_t(0), & \text{if } N = 0. \end{cases} \quad (49)$$

The augmented vector  $\tilde{x}_N(t)$  is composed by the instantaneous state  $x_t(0)$  and the projections of the state function  $x_t$  to the  $N$  first Legendre polynomials. According to Appendix C, an integration by parts allows expressing the time derivative of  $\tilde{x}_N(t)$  as follows

$$\dot{\tilde{x}}_N(t) = H_N \xi_N(t) \quad (50)$$

where

$$\xi_N(t) = \begin{cases} \begin{bmatrix} x_t^T(0) \\ x_t^T(-h) \\ \frac{1}{h} \int_{-h}^0 \mathcal{L}_0(s)x_t(s)ds \\ \vdots \\ \frac{1}{h} \int_{-h}^0 \mathcal{L}_{N-1}(s)x_t(s)ds \end{bmatrix}, & \text{if } N \geq 1 \\ \begin{bmatrix} x_t^T(0) \\ x_t^T(-h) \end{bmatrix}, & \text{if } N = 0 \end{cases} \quad (51)$$

It is worth mentioning that states of the argument system are combined by states of the original delay system and of the Linear time-invariant (LTI) system. Moreover, there is only one delay term in Equation (50) is  $x_t(-h)$ . Therefore, the LKF can be chosen by:

$$V_N(x_t, \dot{x}_t) = \tilde{x}_N^T(t) P_N \tilde{x}_N(t) + \int_{t-h}^t x^T(s) S x(s) ds + h \int_{t-h}^t \int_\theta^t \dot{x}^T(s) R \dot{x}(s) ds d\theta \quad (52)$$

Applying Lemma 5 to Equation (52) yields:

$$V_N(x_t, \dot{x}_t) \geq \tilde{x}_N^T(t) \Theta_N(h) \tilde{x}_N(t) + h \int_{t-h}^t \int_\theta^t \dot{x}^T(s) R \dot{x}(s) ds d\theta \quad (53)$$

The positive definiteness of  $V_N$  is ensured by the condition  $S > 0$ ,  $R > 0$ , and  $\Theta_N(h) > 0$ . Besides,  $\Theta_N(h) > \begin{bmatrix} \varepsilon_1 I & 0 \\ 0 & 0 \end{bmatrix}$  holds for a sufficiently small  $\varepsilon_1 > 0$  which implies that  $V_N(x_t, \dot{x}_t) \geq \varepsilon_1 |x_t(0)|^2$ . Furthermore,

$P_N \prec \lambda \text{diag}(I, I, 3I, 5I, \dots, (2N-1)I)$  holds for a sufficiently large scalar  $\lambda > 0$ . Therefore, it holds:

$$\begin{aligned} V_N(x_t, \dot{x}_t) &\leq \lambda |x_t(0)|^2 + \lambda \sum_{i=0}^{N-1} (2i+1)\Omega_i^T \Omega_i + \int_{t-h}^t x^T(s) S x(s) ds \\ &\quad + h \int_{t-h}^t \int_\theta^t \dot{x}^T(s) R \dot{x}(s) ds d\theta \end{aligned} \quad (54)$$

According to Lemma 5, we get:

$$\begin{aligned} V_N(x_t, \dot{x}_t) &\leq \lambda |x_t(0)|^2 + \int_{t-h}^t x^T(s) (\lambda h I + S) x(s) ds \\ &\quad + h \int_{t-h}^t \int_\theta^t \dot{x}^T(s) R \dot{x}(s) ds d\theta \end{aligned} \quad (55)$$

which guarantees that there exists a scalar  $\varepsilon_2 > 0$ , such that  $V_N(x_t, \dot{x}_t) \leq \varepsilon_2 |\bar{x}_t|_h^2$  holds for  $\forall t > h$ , where  $\bar{x}_t = \begin{bmatrix} x_t \\ \dot{x}_t \end{bmatrix}$ .

Then it holds:

$$\varepsilon_1 |x_t(0)|^2 \leq V_N(x_t, \dot{x}_t) \leq \varepsilon_2 |\bar{x}_t|_h^2. \quad (56)$$

After that, consider the derivative of  $V_N$  for all  $t \geq h$ , we obtain:

$$\begin{aligned} \dot{V}_N(x_t, \dot{x}_t) &= 2\dot{x}_N^T(t) P_N \dot{x}_N(t) + x_t^T(0) S x_t(0) \\ &\quad - x_t^T(-h) S x_t(-h) + h^2 \dot{x}_t^T(0) R \dot{x}_t(0) \\ &\quad - h \int_{-h}^0 \dot{x}_t^T(s) R \dot{x}_t(s) ds. \end{aligned} \quad (57)$$

Substituting  $\tilde{x}_N(t) = G_N(h)\xi_N(t)$ ,  $\dot{\tilde{x}}_N(t) = H_N\xi_N(t)$ , and  $\dot{x}_t(0) = F_N\xi_N(t)$ , we get:

$$\dot{V}_N(x_t, \dot{x}_t) = \xi_N^T(t) \Phi_{N0}(h) \xi_N(t) - h \int_{-h}^0 \dot{x}_t^T(s) R \dot{x}_t(s) ds \quad (58)$$

Applying the Corollary 9 to the order  $N$  and injecting the resulting inequality (24) into Equation (58) leads to:

$$\dot{V}_N(x_t, \dot{x}_t) \leq \xi_N^T(t) \Phi_N(h) \xi_N(t) \quad (59)$$

Hence, if the LMIs (26) are satisfied, there exists a scalar  $\varepsilon_3 > 0$  such that  $\Phi_N(h) \prec \begin{bmatrix} -\varepsilon_3 I & 0 \\ 0 & 0 \end{bmatrix}$ . Therefore, the following inequality holds:

$$\dot{V}_N(x_t, \dot{x}_t) \leq -\varepsilon_3 |x_t(0)|^2, \quad \forall t \geq h \quad (60)$$

The inequality (60) ensures the negative definiteness of  $\dot{V}_N$ . As for the stability of system (21), by integrating inequality (60), we get:

$$V_N(x_t, \dot{x}_t) - V_N(x_h, \dot{x}_h) \leq -\varepsilon_3 \int_h^t |x_s(0)|^2 ds \quad (61)$$

and, hence, Equation (61) yields:

$$\varepsilon_1 |x_t(0)|^2 \leq V_N(x_t, \dot{x}_t) \leq V_N(x_h, \dot{x}_h) \leq \varepsilon_2 |\bar{x}_h|_h^2 \quad (62)$$

Since  $|x_h|_h \leq c_1 |\phi|_h$ ,  $c_1 > 0$  (Hale and Lunel, 2013) and  $|\dot{x}_h|_h \leq c_2 |\phi|_h$ ,  $c_2 > 0$  according to the definition in Equation (21), we obtain that:

$$|x_t(0)|^2 \leq \frac{V_N(x_h, \dot{x}_h)}{\varepsilon_1} \leq c_3 |\phi|_h^2, \quad c_3 > 0 \quad (63)$$

Hence, system (21) is stable. To prove asymptotic stability we note that, for any initial condition  $\phi$ ,  $x$  is uniformly continuous on  $[0, \infty)$  (since  $x$  defined by the right-hand side of system (21) is uniformly bounded). Moreover, Equation (61) yields that  $|x_t(0)|^2$  is integrable on  $[h, \infty)$ . Then, by Barbalat's lemma (Min and Liu, 2007),  $x_t(0) \rightarrow 0$  as  $t \rightarrow \infty$ . Consequently, if the LMI of Theorem are satisfied, the delay system (21) is asymptotically stable for the constant delay  $h$ .

## CRediT authorship contribution statement

**Tiancheng Ruan:** Conceptualization of this study, Methodology, Writing - Original draft preparation, Resources, Software. **Hao Wang:** Formal analysis, Funding acquisition, Supervision, Writing - review & editing. **Linjie Zhou:** Data curation, Investigation. **Yujia Chen:** Writing - Original draft preparation. **Changyin Dong:** Formal analysis, Funding acquisition.

## Acknowledgment

This research was sponsored by the National Science Foundation of China (No. 51878161 and No.52072067), Postgraduate Research & Practice Innovation Program of Jiangsu Province (KYCX22\_0266), Natural Science Foundation of Jiangsu Province (No. BK20210249) and Jiangsu Planned Projects for Postdoctoral Research Funds (No. SBK2021041144).

## References

- Abbas, F., Fan, P., Khan, Z., 2018. A novel low-latency V2V resource allocation scheme based on cellular V2X communications. *IEEE Transactions on Intelligent Transportation Systems* 20, 2185–2197.
- van Arem, B., Abbas, M.M., Li, X., Head, L., Zhou, X., Chen, D., Bertini, R., Mattingly, S.P., Wang, H., Orosz, G., 2016. Integrated traffic flow models and analysis for automated vehicles, in: *Road Vehicle Automation 3*. Springer, pp. 249–258.
- Chang, X., Li, H., Rong, J., Zhao, X., 2020. Analysis on traffic stability and capacity for mixed traffic flow with platoons of intelligent connected vehicles. *Physica A: Statistical Mechanics and its Applications* 557, 124829.
- Chen, T., Wang, M., Gong, S., Zhou, Y., Ran, B., 2021. Connected and automated vehicle distributed control for on-ramp merging scenario: A virtual rotation approach. *Transportation Research Part C: Emerging Technologies* 133, 103451.
- Chin, H., Okuda, H., Tazaki, Y., Suzuki, T., 2015. Model predictive cooperative cruise control in mixed traffic, in: *IECON 2015-41st Annual Conference of the IEEE Industrial Electronics Society*, IEEE, pp. 3199–3205.
- Dey, K.C., Yan, L., Wang, X., Wang, Y., Shen, H., Chowdhury, M., Yu, L., Qiu, C., Soundararaj, V., 2015. A review of communication, driver characteristics, and controls aspects of cooperative adaptive cruise control (CACC). *IEEE Transactions on Intelligent Transportation Systems* 17, 491–509.
- Firooznia, A., Ploeg, J., Van De Wouw, N., Zwart, H., 2017. Co-design of controller and communication topology for vehicular platooning. *IEEE transactions on intelligent transportation systems* 18, 2728–2739.
- Fridman, E., Pila, A., Shaked, U., 2003. Regional stabilization and  $H_\infty$  control of time-delay systems with saturating actuators. *International Journal of Robust and Nonlinear Control: IFAC-Affiliated Journal* 13, 885–907.
- Fu, C., Sayed, T., 2021. Comparison of threshold determination methods for the deceleration rate to avoid a crash (drac)-based crash estimation. *Accident Analysis & Prevention* 153, 106051.
- Ghiasi, A., Hussain, O., Qian, Z.S., Li, X., 2017. A mixed traffic capacity analysis and lane management model for connected automated vehicles: A Markov chain method. *Transportation Research Part B: Methodological* 106, 266–292.
- Gouaisbaut, F., Peaucelle, D., 2006. A note on stability of time delay systems. *IFAC Proceedings Volumes* 39, 555–560.
- Gu, K., Chen, J., Kharitonov, V.L., 2003. Stability of time-delay systems. Springer Science & Business Media.
- Gu, K., Liu, Y., 2009. Lyapunov–Krasovskii functional for uniform stability of coupled differential-functional equations. *Automatica* 45, 798–804.
- Hale, J.K., Lunel, S.M.V., 2013. Introduction to functional differential equations. volume 99. Springer Science & Business Media.
- Hengster-Movric, K., Lewis, F.L., Šebek, M., Vyhlídal, T., 2015. Cooperative synchronization control for agents with control delays: A synchronizing region approach. *Journal of the Franklin Institute* 352, 2002–2028.
- Hu, Y., Chen, C., He, J., Yang, B., 2021. Eco-platooning for cooperative automated vehicles under mixed traffic flow. *IEEE Transactions on Intelligent Transportation Systems* 22, 2023–2034.
- Jin, I.G., Orosz, G., 2016. Optimal control of connected vehicle systems with communication delay and driver reaction time. *IEEE Transactions on Intelligent Transportation Systems* 18, 2056–2070.
- Lee, W.I., Lee, S.Y., Park, P., 2018. Affine Bessel–Legendre inequality: Application to stability analysis for systems with time-varying delays. *Automatica* 93, 535–539.
- Martín-Sacristán, D., Roger, S., Garcia-Roger, D., Monserrat, J.F., Spapis, P., Zhou, C., Kaloxyllos, A., 2020. Low-Latency Infrastructure-Based Cellular V2V Communications for Multi-Operator Environments With Regional Split. *IEEE Transactions on Intelligent Transportation Systems* 22, 1052–1067.
- Milanés, V., Shladover, S.E., 2014. Modeling cooperative and autonomous adaptive cruise control dynamic responses using experimental data 48, 285–300. doi:10.1016/j.trc.2014.09.001.
- Min, Y.Y., Liu, Y.G., 2007. Barbalat lemma and its application in analysis of system stability. *Journal of Shandong University (engineering science)* 37, 51–55.
- Montanino, M., Punzo, V., 2021. On string stability of a mixed and heterogeneous traffic flow: A unifying modelling framework. *Transportation Research Part B: Methodological* 144, 133–154.
- Monteil, J., Bourdache, M., Leith, D.J., 2019. L 2 and L  $\infty$  Stability Analysis of Heterogeneous Traffic With Application to Parameter Optimization for the Control of Automated Vehicles. *IEEE Transactions on Control Systems Technology* 27, 934–949. doi:10.1109/TCST.2018.2808909.
- Navas, F., Milanés, V., 2019. Mixing V2V- and non-V2V-equipped vehicles in car following. *Transportation Research Part C: Emerging Technologies* 108, 167–181. URL: <https://doi.org/10.1016/j.trc.2019.08.021>, doi:10.1016/j.trc.2019.08.021.

- Navas, F., Milanés, V., Nashashibi, F., 2016. Using Plug&Play Control for stable ACC-CACC system transitions, in: 2016 IEEE Intelligent Vehicles Symposium (IV), IEEE. pp. 704–709.
- Park, P., Lee, W.I., Lee, S.Y., 2015. Auxiliary function-based integral inequalities for quadratic functions and their applications to time-delay systems. *Journal of the Franklin Institute* 352, 1378–1396.
- Pirani, M., Baldi, S., Johansson, K.H., 2022. Impact of Network Topology on the Resilience of Vehicle Platoons. *IEEE Transactions on Intelligent Transportation Systems*.
- Qin, Y., Wang, H., Ran, B., 2018. Stability Analysis of Connected and Automated Vehicles to Reduce Fuel Consumption and Emissions. *Journal of Transportation Engineering, Part A: Systems* 144, 04018068. doi:10.1061/jtpebs.0000196.
- Ruan, T., Wang, H., Zhou, L., Zhang, Y., Dong, C., Zuo, Z., 2022. Impacts of information flow topology on traffic dynamics of cav-mv heterogeneous flow. *IEEE Transactions on Intelligent Transportation Systems*, 1–16doi:10.1109/TITS.2022.3170965.
- Ruan, T., Zhou, L., Wang, H., 2021. Stability of heterogeneous traffic considering impacts of platoon management with multiple time delays. *Physica A: Statistical Mechanics and its Applications* 583, 126294.
- Saccoccia, F.F., Cunto, F., Guido, G., Vitale, A., 2008. Comparing safety at signalized intersections and roundabouts using simulated rear-end conflicts. *Transportation Research Record* 2078, 90–95.
- Sarker, A., Shen, H., Rahman, M., Chowdhury, M., Dey, K., Li, F., Wang, Y., Narman, H.S., 2019. A review of sensing and communication, human factors, and controller aspects for information-aware connected and automated vehicles. *IEEE transactions on intelligent transportation systems* 21, 7–29.
- Schrank, D., Eisele, B., Lomax, T., 2012. TTI's 2012 urban mobility report. Texas A&M Transportation Institute. The Texas A&M University System 4.
- Seuret, A., Gouaisbaut, F., 2013. Wirtinger-based integral inequality: application to time-delay systems. *Automatica* 49, 2860–2866.
- Stüdli, S., Seron, M.M., Middleton, R.H., 2017. From vehicular platoons to general networked systems: String stability and related concepts. *Annual Reviews in Control* 44, 157–172.
- Thota, J., Abdullah, N.F., Doufexi, A., Armour, S., 2019. V2V for vehicular safety applications. *IEEE Transactions on Intelligent Transportation Systems* 21, 2571–2585.
- Verizon North, L.L.C., 2020. Federal Communications Commission. Proceeding Number 19, 354.
- Vu, H.V., Liu, Z., Nguyen, D.H.N., Morawski, R., Le-Ngoc, T., 2020. Multi-agent reinforcement learning for joint channel assignment and power allocation in platoon-based C-V2X systems. arXiv preprint arXiv:2011.04555 .
- Vukadinovic, V., Bakowski, K., Marsch, P., Garcia, I.D., Xu, H., Sybis, M., Sroka, P., Wesolowski, K., Lister, D., Thibault, I., 2018. 3GPP C-V2X and IEEE 802.11p for Vehicle-to-Vehicle communications in highway platooning scenarios. *Ad Hoc Networks* 74, 17–29. doi:10.1016/j.adhoc.2018.03.004.
- Wang, J., Zheng, Y., Chen, C., Xu, Q., Li, K., 2021. Leading cruise control in mixed traffic flow: System modeling, controllability, and string stability. *IEEE Transactions on Intelligent Transportation Systems* .
- Wang, M., Hoogendoorn, S.P., Daamen, W., van Arem, B., Shyrokau, B., Happee, R., 2018. Delay-compensating strategy to enhance string stability of adaptive cruise controlled vehicles. *Transportmetrica B* 6, 211–229. URL: <https://doi.org/10.1080/21680566.2016.1266973>, doi:10.1080/21680566.2016.1266973.
- Wang, Z., Bian, Y., Steven E. Shladover, 2019. A survey on cooperative longitudinal motion control of multiple connected and automated vehicles. *IEEE INTELLIGENT TRANSPORTATION SYSTEMS MAGAZINE* 12, 4–24. doi:10.3969/j.issn.1001-0505.2020.05.024.
- Wei, Y., Avci, C., Liu, J., Belezamo, B., Aydin, N., Li, P.T., Zhou, X., 2017. Dynamic programming-based multi-vehicle longitudinal trajectory optimization with simplified car following models. *Transportation research part B: methodological* 106, 102–129.
- Wilson, R.E., Ward, J.A., 2011. Car-following models: Fifty years of linear stability analysis - a mathematical perspective. *Transportation Planning and Technology* 34, 3–18. doi:10.1080/03081060.2011.530826.
- Ye, L., Yamamoto, T., 2018. Impact of dedicated lanes for connected and autonomous vehicle on traffic flow throughput. *Physica A: Statistical Mechanics and its Applications* 512, 588–597.
- Yu, H., Jiang, R., He, Z., Zheng, Z., Li, L., Liu, R., Chen, X., 2021. Automated vehicle-involved traffic flow studies: A survey of assumptions, models, speculations, and perspectives. *Transportation research part C: emerging technologies* 127, 103101.
- Zheng, Y., Li, S.E., Wang, J., Cao, D., Li, K., 2015. Stability and scalability of homogeneous vehicular platoon: Study on the influence of information flow topologies. *IEEE Transactions on intelligent transportation systems* 17, 14–26.
- Zhong, Z., Lee, E.E., Nejad, M., Lee, J., 2020. Influence of CAV clustering strategies on mixed traffic flow characteristics: An analysis of vehicle trajectory data. *Transportation Research Part C: Emerging Technologies* 115, 102611.
- Zhou, L., Ruan, T., Ma, K., Dong, C., Wang, H., 2021. Impact of CAV platoon management on traffic flow considering degradation of control mode. *Physica A: Statistical Mechanics and its Applications* 581, 126193.
- Zhou, Y., Ahn, S., 2019. Robust local and string stability for a decentralized car following control strategy for connected automated vehicles. *Transportation Research Part B: Methodological* 125, 175–196.
- Zhou, Y., Ahn, S., Wang, M., Hoogendoorn, S., 2020. Stabilizing mixed vehicular platoons with connected automated vehicles: An H-infinity approach. *Transportation Research Part B: Methodological* 132, 152–170.
- Zhou, Y., Wang, M., Ahn, S., 2019. Distributed model predictive control approach for cooperative car-following with guaranteed local and string stability. *Transportation research part B: methodological* 128, 69–86.
- Zhu, Y., He, H., Zhao, D., 2019. LMI-based synthesis of string-stable controller for cooperative adaptive cruise control. *IEEE Transactions on Intelligent Transportation Systems* 21, 4516–4525.